Dielectronic recombination of U^{28+} atomic ions

D. M. Mitnik, M. S. Pindzola, and F. Robicheaux
Department of Physics, Auburn University, Auburn, Alabama

N. R. Badnell
Department of Physics and Applied Physics, University of Strathclyde, Glasgow, Scotland

O. Uwira, A. Müller, A. Frank, J. Linkemann,* and W. Spies[†]
Institut für Kernphysik, Strahlenzentrum, Universität Gießen, Gießen, Germany

N. Angert and P. H. Mokler
Gesellschaft für Schwerionenphysik, Darmstadt, Germany

R. Becker and M. Kleinod
Institut für Angewandte Physik, Universität Frankfurt, Frankfurt, Germany

S. Ricz
Institute of Nuclear Research, Debrecen, Hungary

L. Empacher[‡]
Institut für Strahlenphysik, Universität Stuttgart, Stuttgart, Germany

Dielectronic recombination cross sections for U^{28+} are calculated in the distorted-wave approximation and compared with measurements obtained using an electron-ion merged beams apparatus. Although the experiment covered energies between 0 and 420 eV, the theoretical calculations were restricted to energies below 180 eV, where the most important resonance structures occur. The theoretical cross sections involving $\Delta n = 0$ excitations from the $5s^2 5p^2$ ground configuration are found to be equally well described using either semirelativistic wave functions, as found in the AUTOSTRUCTURE codes, or fully relativistic wave functions, as found in the HULLAC codes. The main features of the experimental spectrum are well identified for the 80–180 eV energies, although complicated by the possible presence of unknown fractions of metastable levels. However, the resonance structures observed at the energies less than 80 eV, in the vicinity of a huge zero-energy peak, remain largely unexplained. [S1050-2947(98)00806-3]

PACS number(s): 34.80.Lx

I. INTRODUCTION

Since the early experimental measurements of dielectronic recombination (DR) in the early middle 1980s, the development of ion accelerators, traps, and storage rings has made possible the observation of increasingly more detailed and complex DR spectra, which in turn has challenged the most sophisticated theoretical computations for interpretation [1,2]. For example, there have been recent studies of recombination in fluorinelike ($2s^2 2p^5$) selenium [3], lithiumlike ($1s^2 2s$) argon [4], and fluorinelike iron [5]. In each study resonance structures were measured and calculated at high resolution over a wide energy range. Part of the drive to move to more complex DR spectra has been the demand by astrophysical and laboratory plasma modelers for accurate

DR rate coefficients for many L-shell and even some M-shell atomic ions.

In this paper we report on theoretical calculations and experimental measurements of a very complicated O-shell dielectronic recombination spectrum for U^{28+}, whose ground configuration is $5s^2 5p^2$. Although the step from L shell to O shell is too large to hope for a detailed agreement between theory and experiment, we do identify the major Rydberg series. The interest in U^{28+} comes from earlier single-pass merged-beam experiments at the Universal Linear Accelerator (UNILAC) of Gesellschaft für Schwerionenphysik (GSI) in which a huge recombination peak at zero energy was discovered [6]. It may prove helpful in explaining the nature of the zero-energy peak, if the dielectronic recombination spectrum that contributes to the huge peak is better understood, even at a qualitative level. The huge peak has also been found in other complex atomic systems. The remaining sections of this paper are arranged as follows. Section II contains a review of the basic DR formulas and computational methods. Section III describes the present high-resolution DR measurements. Section IV compares semirelativistic and fully relativistic distorted-wave calculations for U^{28+} with

---

*Present address: Basler GmbH, Ahrensburg, Germany.

[†]Present address: Department of Atomic Physics, Stockholm University, S-104 05 Stockholm, Sweden.

[‡]Present address: Institut für Plasmaforschung, Universität Stuttgart, Stuttgart, Germany.

each other and with the present observations. Section V contains a brief summary of our findings.

II. THEORY

In the isolated-resonance and independent-processes approximation, the energy-averaged dielectronic recombination cross section for a given initial level i through an intermediate level j is given by [7]

$$\bar{\sigma}(i \rightarrow j) = \frac{(2\pi a_0 I)^2 \tau_0}{E_c \Delta E_c} \frac{g_j}{2g_i} A_a(j \rightarrow i)$$
$$\times \left[\frac{\sum_k A_r(j \rightarrow k)}{\sum_m A_a(j \rightarrow m) + \sum_n A_r(j \rightarrow n)} \right]. \quad (1)$$

Here E_c is the energy of the continuum electron, which is fixed by the position of the resonances, ΔE_c is an energy bin width, g_j is the statistical weight of the $(N+1)$-electron ion doubly excited level, g_i is the statistical weight of the N-electron ion initial target level, I is the ionization potential energy of hydrogen, and a_0 and τ_0 are the atomic units for length and time, respectively $[(2\pi a_0)^2 \tau_0 = 2.6741 \times 10^{-32}$ cm^2 s]. The denominator of the term in square brackets is the total decay rate of the intermediate resonance level j. It consists of a sum of the radiative rates A_r and a sum of the autoionization rates A_a over all possible levels. In the numerator, the sum over k is taken, for simplicity, over all levels that are stable against autoionization. The term in the square brackets is called the branching ratio for radiative recombination.

The various rates entering Eq. (1) are calculated using the AUTOSTRUCTURE package [8,9]. The calculations may be performed in a perturbative-relativistic intermediate-coupling mode using a Breit-Pauli Hamiltonian that includes both one-body and two-body fine-structure interactions. For application to highly charged ions, the code uses a semirelativistic procedure, following the work of Cowan and Griffin [10], in which the mass-velocity and Darwin operators have been added into the nonrelativistic Hartree-Fock differential equations. Perturbation theory is then used to evaluate the remaining one-body and two-body fine-structure interactions. The various rates entering Eq. (1) are also calculated using the HULLAC package [11], based on the RELAC code [12]. The calculations are performed in a fully relativistic intermediate-coupling mode based on a parametric potential for the Dirac Hamiltonian. The main idea of the parametric potential method is the introduction of a central potential as an analytic function of screening parameters that are determined by minimizing the first-order relativistic energy of a set of configurations. This optimized potential is used to calculate all one-electron orbitals and energies, relativistic multiconfiguration bound states and their energies, continuum orbitals, and all the required transition rates.

In order to compare the theory with the experimental data, we calculated the rate coefficient

$$\langle v \sigma \rangle = \int_0^\infty v \sigma(v) f(v) dv, \quad (2)$$

where v is the electron velocity and $f(v)$ is the electronic velocity distribution. For an ordinary gas of electrons at a given temperature, one would describe the velocity distribution by a three-dimensional Maxwellian distribution. However, due to the longitudinal acceleration of the electron beam in our experiment, the three-dimensional symmetry is broken. Therefore, the relative velocity spread in the experiment cannot be characterized by a single temperature. This results in two different temperatures: $T_\perp$ associated with the two-dimensional motion perpendicular to the beam direction and $T_\parallel$ associated with the one-dimensional motion parallel to the beam direction. The relative velocity distribution then becomes

$$f(v) = \frac{m_e}{2\pi k T_\perp} e^{-m_e v_\perp^2 / 2k T_\perp} \left[\frac{m_e}{2\pi k T_\parallel} \right]^{1/2} e^{-m_e (v_\parallel - \Delta)^2 / 2k T_\parallel}, \quad (3)$$

where m_e is the mass of the electron, $v_\perp$ and $v_\parallel$ are the electron-velocity components perpendicular and parallel to the ion-beam direction, respectively, and Δ is the detuning velocity that defines the relative energy ($\frac{1}{2} m_e \Delta^2$).

III. EXPERIMENT

The present measurements were carried out at the UNILAC heavy-ion accelerator facility of the GSI in Darmstadt. The experimental setup and the procedures of rate measurements at the electron target of the UNILAC have been described in great detail elsewhere [13]. In this experiment ^{238}U^{28+} ions were accelerated to 5.96 MeV/amu and then transported into the electron target through an energy-selective beam line. The resulting ion beam available for our experiments had a relative energy spread of less than 10^{-4}. The total flight time of the ions from the location of their production to the electron-ion interaction region was about 4 μs, during which many of the excited states of the ions populated in the production process had a good chance to decay. The collimated U^{28+} ion beam with electrical currents of typically 10 nA was merged with a 3-mm-diam electron beam at densities between $n_e = 4.9$ and 6.0×10^8 cm^{-3}. It was experimentally ensured that the ion beam was fully immersed in the uniform-density electron beam over the whole length of 42.5 cm of the interaction region. The gun of the electron target was operated in its low-perveance mode, which was associated with a magnetic guiding field for the electrons of $B = 5.3 \times 10^{-3}$ T$\sqrt{U_c/V}$, where U_c is the electron acceleration voltage. The magnetic field was produced by a superconducting solenoid with correction windings providing a field homogeneity in the interaction region of electrons and ions within relative deviations of less than 10^{-4}. Typical numbers for U_c and the related magnetic field B are $U_c = 3$ kV and $B = 0.29$ T. Parent ions and recombined product ions emerging from the electron target were separated by a magnet and focused to different detectors, 3.3 cm apart from each other. The recombined ions were detected by a position-sensitive single-particle detector while the parent ions were collected in a wide Faraday cup. Normalized re-
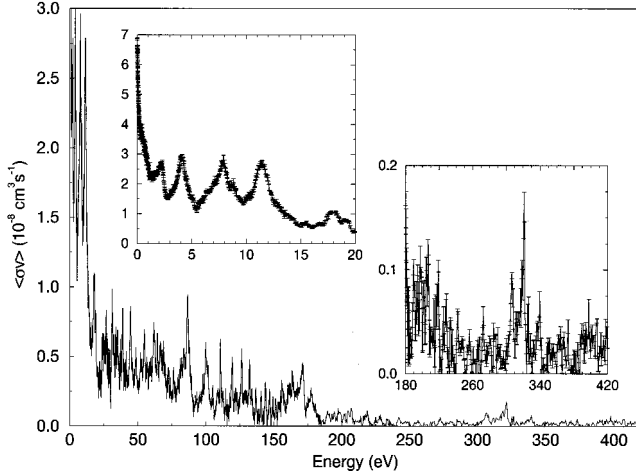
FIG. 1. Measured recombination rate coefficient for U^{28+} ions from 0 eV to 420 eV. The two insets show the DR resonances from 0 eV to 20 eV and from 180 eV to 350 eV on adjusted scales. The middle part of the spectrum is shown on an expanded scale in subsequent figures. Statistical uncertainties are indicated.

combination rates α were determined from

$$\alpha = \frac{R\gamma^2 v_i qe}{I_i \ell_{eff} n_e \epsilon},\tag{4}$$

where R is the observed counting rate of recombined ions, γ the relativistic Lorentz factor, v_i the velocity of the ions, $qe = 28e$ the charge of the ions, I_i the ion beam current, $\ell_{eff} = 42.5$ cm the effective interaction length, n_e the electron density, and $\epsilon = 1$ the detector efficiency. The overall relative systematic uncertainty of the measured rate α was calculated as the square root of the sum of the squared relative uncertainties of the quantities entering Eq. (4). It amounts to $\Delta\alpha/\alpha = \pm 26\%$. The experimental error bars shown in this paper are the statistical uncertainties $\Delta\alpha_{st}$ only. The total most probable uncertainty of a measurement of α is determined by

$$\frac{\Delta\alpha_{tot}}{\alpha} = \sqrt{\left(\frac{\Delta\alpha}{\alpha}\right)^2 + \left(\frac{\Delta\alpha_{st}}{\alpha}\right)^2}.\tag{5}$$

The electron beam in this experiment was relatively dense compared to electron-cooling facilities at heavy-ion storage rings, but at the same time it was quite cold and thus allowed the measurement of recombination rates with a good energy resolution. For variation of the electron-ion interaction energy the electron energy in the laboratory frame was changed. The latter was defined by the cathode voltage U_c, the voltage U_{int} applied to a set of two coaxial parallel plate electrodes (separated by 30 mm), and the space-charge potential in the interaction region. The voltage U_{int} was changed from -200 V to -600 V, measured from the ground potential, in up to 1024 equidistant steps. The voltage U_c was changed from -3650 V to -2150 V in steps of typically 300 V so that scans of U_{int} provided overlapping energy bins between approximately 1550 eV and 3450 eV. The space-charge potential of the electron beam, centered between the two parallel plates, can be calculated approximately (in V) as

$$U(r=0) = U_{int} - 0.17\frac{I_e[\text{mA}]}{\beta}.\tag{6}$$

From the electron beam currents and energies a potential depression by the electron space charge of at most 30 eV at 3200 eV can be calculated (about 5 eV in the electron beam itself). This potential shift on the axis of the electron beam reduces to at most 20 eV at 2000 eV. Since the plate electrodes in the actual experiment have finite extension, a closed-trap potential distribution is formed for slow ions produced in the interaction region. These ions partially compensate the electron space charge and thus reduce the shift of electron energies discussed above. As an example, the ion velocity at 5.96 MeV/amu is matched with that of electrons with 3270 eV. Without space-charge potentials this would correspond to an electron acceleration voltage $\Delta U = |U_c - U_{int}| = 3270$ V. Considering the full electron space charge, the matching condition is expected at $\Delta U = 3300$ V on the electron beam axis. We observed $\Delta U = 3278$ V, indicating that up to 73% of the electron space charge may be compensated by slow trapped ions. Since we could not experimentally control the amount of the space-charge compensation in each individual energy scan, the energy scale of the measurements contains an uncertainty. The transformation of the electron laboratory energies (with the above uncertainties) into the center-of-mass frame leads to possible energy shifts of only 0.1 eV at $E_{cm} = 1$ eV and up to about 10 eV at $E_{cm} = 180$ eV. In Fig. 1 we show an overview over the measured U^{28+} recombination spectrum from 0 eV to 420 eV. The dominant feature is the recombination peak at zero electron-ion collision energy. The size and energy dependence of this peak coincide with our previous measurement [6]. The structures in the spectrum at higher energies are small compared to the zero-energy peak. Therefore, two insets in the figure are used to show the DR resonances on adjusted scales. The peaks extending from 0 eV to 20 eV shown in the left inset are still huge compared to typical DR resonances (such as those found with Se^{25+} [3]). The features beyond 180 eV shown in the right inset are small and were measured with relatively poor statistics. Background corrections of this part of the spectrum are difficult and lead to additional uncertainties. The middle part of the experimental spectrum is shown on an expanded scale in subsequent figures.

IV. RESULTS

A. Comparison between semirelativistic and fully relativistic calculations

We calculated the bound-state energy spectrum of U^{28+} using several different theoretical methods. First, a multiconfiguration Hartree-Fock method including relativistic corrections through the Breit-Pauli approximation [14] was applied. Then the AUTOSTRUCTURE codes, both in the perturbative-relativistic mode (AS-PR) and in the semi-relativistic mode (AS-SR), were used. Table I shows the energies of the 27 levels of the lowest three configurations of U^{28+}: $5s^25p^2$, $5s5p^3$, and $5s^25p5d$, calculated by using these different methods.
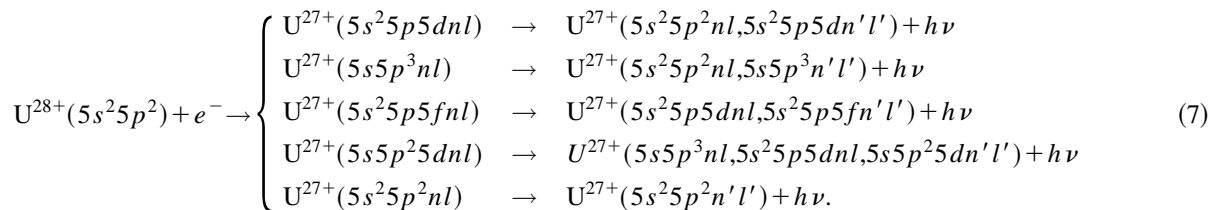
TABLE I. Calculated energies of the lowest three configurations in U^{28+} calculated by using a multiconfiguration Hartree-Fock method (MCHF), the AUTOSTRUCTURE code in the perturbative-relativistic [AS (PR)] and in the semirelativistic [AS (SR)] mode, and the HULLAC code.

Level	Configuration	Term	Energy (eV)			
			MCHF	AS (PR)	HULLAC	AS (SR)
1	$5s^25p^2$	$^3P_0$	0.0000	0.0000	0.0000	0.0000
2	$5s^25p^2$	$^3P_1$	45.552	46.256	65.884	68.423
3	$5s^25p^2$	$^1D_2$	48.452	49.147	68.876	71.504
4	$5s5p^3$	$^3D_2$	150.52	150.57	131.80	135.43
5	$5s^25p^2$	$^3P_2$	96.169	97.554	137.24	142.22
6	$5s5p^3$	$^3D_1$	118.90	118.15	142.05	145.61
7	$5s^25p^2$	$^1S_0$	102.36	103.70	143.60	148.66
8	$5s^25p5d$	$^3F_2$	108.77	108.05	170.33	165.86
9	$5s^25p5d$	$^3D_1$	161.65	161.45	182.26	178.40
10	$5s^25p5d$	$^1D_2$	223.37	223.87	186.37	184.44
11	$5s^25p5d$	$^3F_3$	171.78	171.54	188.07	185.06
12	$5s5p^3$	$^5S_2$	151.29	151.24	198.49	203.17
13	$5s5p^3$	$^3D_3$	156.42	156.48	202.91	208.30
14	$5s5p^3$	$^3P_0$	162.59	162.62	205.43	211.92
15	$5s5p^3$	$^1P_1$	207.27	207.86	210.77	216.90
16	$5s5p^3$	$^1D_2$	173.49	173.19	212.50	218.36
17	$5s5p^3$	$^3S_1$	171.46	171.35	213.51	219.85
18	$5s^25p5d$	$^3D_2$	208.04	208.59	247.30	245.96
19	$5s5p^3$	$^3P_1$	167.85	167.83	287.25	246.46
20	$5s^25p5d$	$^1F_3$	209.68	210.18	248.65	246.53
21	$5s^25p5d$	$^3P_0$	208.88	209.43	248.40	246.60
22	$5s^25p5d$	$^3F_4$	212.75	213.33	252.64	251.18
23	$5s^25p5d$	$^3P_2$	168.79	168.77	254.29	253.89
24	$5s^25p5d$	$^3D_3$	226.03	226.39	266.20	264.64
25	$5s^25p5d$	$^1P_1$	230.48	230.85	248.08	265.57
26	$5s5p^3$	$^3P_2$	204.91	205.68	277.93	285.79
27	$5s^25p5d$	$^3P_1$	220.79	221.41	266.67	295.97

The large discrepancies between the AS-PR and AS-SR calculations indicate the presence of strong relativistic effects. Therefore, our semirelativistic calculations were compared with fully relativistic calculations obtained using the HULLAC codes. A comparison of the energies of the last two columns in Table I shows that there is good general agreement between the semirelativistic and the fully relativistic calculations. There is a small difference of about 4 eV in the average configuration energies. Some levels are strongly mixed and the dominant *LSJ* designation for a given energy is different for the two calculations (see, for example, levels 19, 25, and 27 in Table I). Other than these discrepancies in labeling, the energies of the levels relative to the average configuration energies are in agreement in the two calculations.

The main DR reaction pathways for $\Delta n = 0$ excitation from the ground configuration of U^{28+} are given by
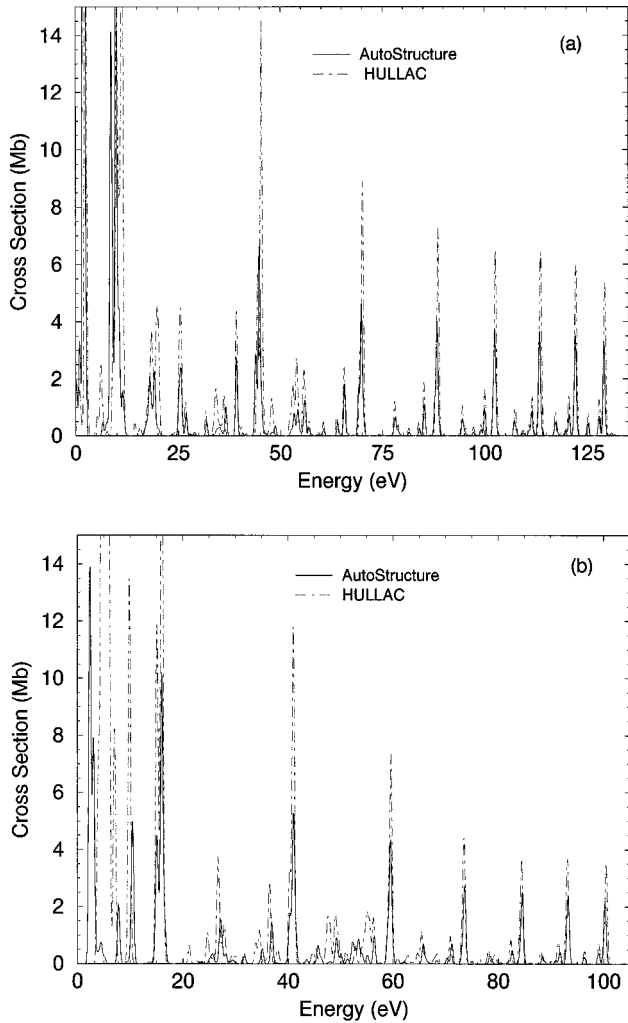
$$U^{28+}(5s^25p^2) + e^- \rightarrow \begin{cases} U^{27+}(5s^25p5dnl) & \rightarrow & U^{27+}(5s^25p^2nl, 5s^25p5dn'l') + h\nu \\ U^{27+}(5s5p^3nl) & \rightarrow & U^{27+}(5s^25p^2nl, 5s5p^3n'l') + h\nu \\ U^{27+}(5s^25p5dfnl) & \rightarrow & U^{27+}(5s^25p5dnl, 5s^25p5fn'l') + h\nu \\ U^{27+}(5s5p^25dnl) & \rightarrow & U^{27+}(5s5p^3nl, 5s^25p5dnl, 5s5p^25dn'l') + h\nu \\ U^{27+}(5s^25p^2nl) & \rightarrow & U^{27+}(5s^25p^2n'l') + h\nu. \end{cases} \quad (7)$$

FIG. 2. Calculated DR cross section through the (a) $5s^2 5p 5dnl$ ($n=6-15$), and (b) $5s 5p^3 nl$ ($n=6-15$) intermediate configurations. The results were energy averaged over 0.1 width bins and convoluted with a 0.5-eV-width (FWHM) Gaussian. The solid line shows the results by using the AUTOSTRUCTURE code and the dashed line the results by using HULLAC code.

For the DR channels listed in Eq. (7), the principal contribution is given by the complexes having principal quantum number of about 10. For these intermediate configurations having energies greater than the first ionization limit, the majority of the Rydberg levels are allowed to autoionize. As an illustration of the order of magnitude of the calculations for such complexes with $n=10$, the first three channels listed in Eq. (7) have the following number of levels: 1016 for the $5s^2 5p 5d 10l$ ($l=0-9$), 702 for the $5s^2 5p^3 10l$ ($l=0-9$), and 1352 levels for the $5s^2 5p 5f 10l$ ($l=0-9$) complex.

Figure 2(a) shows the results of the calculation of the DR cross section through the most important $5s^2 5p 5dnl$ ($n=6-15$) double-excited intermediate levels, calculated by using the AUTOSTRUCTURE codes. The cross sections are energy averaged over energy bins having a 0.1 eV width and then convoluted by a 0.5-eV-width [full width at half maximum (FWHM)] Gaussian. For comparison, the results obtained by the use of the HULLAC codes are also shown in Fig. 2(a). Taking into account that the calculated energies of the peaks are the results of the calculations of the energy levels

of two different ions, the overall error of the theoretical energy results is of about 5 eV. In order to facilitate the comparison, the results obtained in this last calculation were shifted toward the lower energies, by 4.5 eV. The comparison shows very good agreement.

For the low components of the $5s^2 5p 5dnl$ series ($n \leqslant 9$), the distance between the l peaks is so large that the n complexes overlap. For the higher-n complexes, beginning at around $E=60$ eV, the distance between the l peaks is smaller and the same pattern is recognizable for each n complex. At lower energies the height of the peaks is larger due to the factor E_c in the denominator of Eq. (1). As the electron energy increases this factor in the denominator becomes larger and causes the cross section to decrease. Another factor that produces a decrease in the cross section as the n quantum number increases is the decrease in the autoionization rates (roughly proportional to n^{-3}). However, near the threshold of the series, the convoluted cross section begins to increase again and this is a consequence of the accumulation of many resonances in a narrow energy range.

The next most important contribution to the DR cross section is the complex $5s 5p^3 nl$. Figure 2(b) shows the calculated DR cross section through the intermediate $5s 5p^3 nl$ ($n=6-15$) configurations, calculated using both methods described above. For this case, again, the agreement is very good. However, here the results obtained by using the HULLAC codes were now shifted in the opposite direction by 4.0 eV. The good agreement obtained between both methods justifies the use of the computationally less demanding semi-relativistic method for the total DR calculation.

B. Comparison between theory and experiment

The starting point for the understanding of an experimental DR spectrum consists in the identification of the thresholds energies for the different channels. Having identified the threshold of a series, it is possible to predict the position of the rest of the peaks of this series, assuming that for high-n quantum numbers, the contribution to DR comes mainly from the accumulation of levels with high-l quantum angular numbers, which have a small quantum defect. Therefore, a hydrogenic approximation could be taken for the calculation of the energy levels.

In principle, one should observe an infinite series of resonances associated with each individual core excitation, ending at the respective threshold energies. These threshold energies should correspond to the recombining ion energy levels. However, the presence of strong analyzing fields acting on the ions outside the interaction region in the experiment reduces the maximum number of Rydberg states to a finite value. Therefore, the position of the threshold energies and the recombining ion energy levels may be slightly different. Moreover, a variety of experimental effects can produce uncertainties of about 5% in the apparent position of the resonances. In general, since the experimental spectrum consists of several single scans and for every scan the energy calibration is slightly different, the identification of the resonances by their energy can be a very difficult task. In some cases, the different series are overlapped and they are hardly recognizable.

For the cases in which, for the reasons enumerated above, there is not clear evidence of the position of any threshold limit, we have developed the following threshold identification method. First we assign to each resonance of a particular Rydberg series a principal quantum number n. The resonance will be located in the spectrum at an energy E_n given by (in atomic units)

$$E_n = E_T - \frac{q^2}{2} \frac{1}{(n+\mu)^2} = E_T - \frac{q^2}{2} \frac{1}{\nu^2}, \qquad (8)$$

where E_T is the threshold energy of the Rydberg series, q denotes the charge of the ion, μ is the quantum defect, and ν is the effective quantum number. The idea is to express the effective quantum number as a function of the incident electron energy E and the threshold energy E_T,

$$\nu(E, E_T) = \frac{q}{\sqrt{2(E_T - E)}}. \qquad (9)$$

We then transform the DR cross section from the incident energy domain to the threshold energy domain:

$$F(E_T) = \int_{E_{min}}^{E_{max}} \sigma^{DR}(E) e^{i2\pi\nu(E,E_T)} \frac{\partial\nu}{\partial E} dE, \qquad (10)$$

where E_{min} must be any energy value lower than a possible threshold energy. For an ideal experiment, the integral must be calculated from $E_{min} = 0$ to $E_{max} = E_T$. However, in applying this equation, care must be taken for points near the threshold energy due to the singularity in the density of states. For this case, the integral becomes a sum of only the last few terms, dominated by large weight factors multiplying the differential and having a meaningless large phase value in the exponent. Therefore, the integral must be cut off at a point $E_{max} < E_T$ where, for an energy interval equal to the experimental resolution ΔE_{expt}, the difference in the phase will be less than one. If we require $\Delta\nu_{max} \leqslant 1/2$, then

$$\Delta\nu_{max} = \frac{\partial\nu}{\partial E} \Delta E_{expt} \leqslant \frac{1}{2} \qquad (11)$$

and we obtain

$$E_{max} = E_T - \left[\frac{q\Delta E_{expt}}{\sqrt{2}} \right]^{2/3}. \qquad (12)$$

This transformation produces a peak in the spectrum, at every threshold value for which the peaks are spaced by the ν^{-2} behavior given in Eq. (8).

We now apply the threshold identification method to the particularly complicated case of U^{28+}. Figure 3(a) shows the DR experimental spectrum as a function of incident energy in the range 0–180 eV, while Fig. 3(b) shows the transformed DR spectrum. The transformed spectrum shows that there is only one clear Rydberg series, which has a threshold energy of about 173 eV. There are many other peaks, but they are not much bigger than the surrounding background.
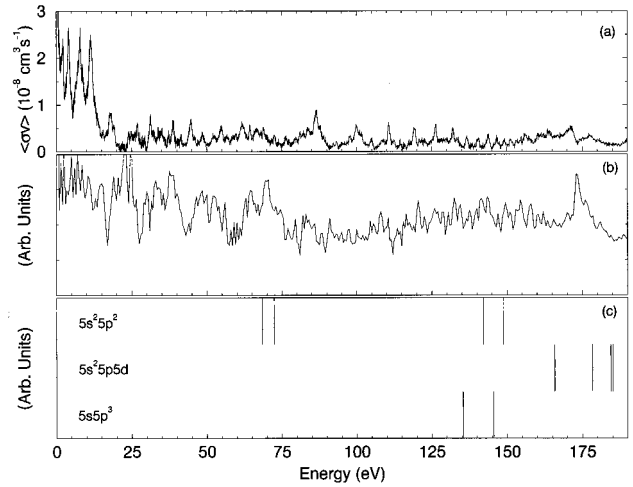

FIG. 3. (a) Experimental data of the U^{28+} dielectronic recombination rate coefficient $\langle\sigma v\rangle$, as a function of the electron energy, for 5.94 MeV/amu. (b) Threshold transform of the experimental spectrum. (c) Energy spectrum of the Gd-like uranium ion.

Thus the analysis indicates that there is only one dominant channel and in order to identify it, we show in Fig. 3(c) the low-lying bound energy levels of U^{28+} belonging to the configurations $5s^25p^2$, $5s^25p5d$, and $5s5p^3$. The dominant channel must have a bound level of U^{28+} immediately above the threshold energy of 173 eV and we identify this level as $5s^25p5d\ ^3D_1$ [or $5s^25p_{1/2}5d_{3/2}(J=1)$ in jj coupling]. The $5s5p^3nl$ channel has a couple of bound levels of U^{28+} around 140 eV, but the peak in the transformed spectrum is not easily recognizable, due to the presence of a strong background at this energy region. The broad peak observed in the transformed spectrum [Fig. 3(b)] around 70 eV suggests the possibility of another contribution in the DR spectra given by the $5s^25p^2nl$ intermediate channel, but as it is explained below, this contribution was not included in the calculations.

Having identified the major series, we present the results of the total DR rate coefficient $\langle v\sigma\rangle$ calculations from the
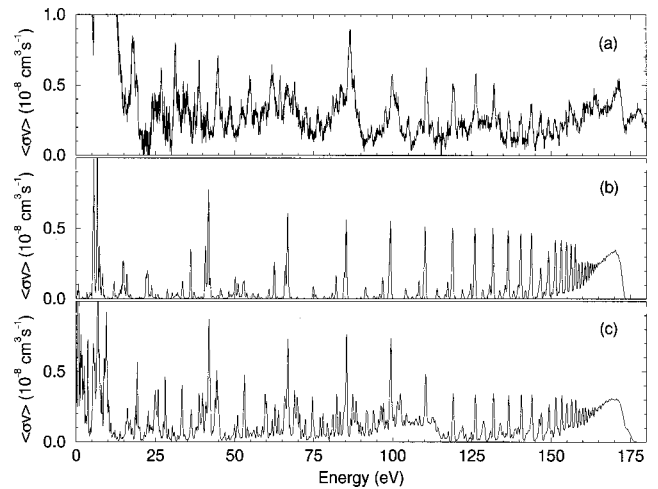

FIG. 4. DR total rate coefficient. (a) Experimental results. (b) Calculated results assuming that only the ground state is populated. (c) Calculated results assuming a statistical population for the first three levels. The temperatures $kT_\perp = 0.1$ eV and $kT_\parallel = 1$ meV were used in the calculation of $\langle\sigma v\rangle$.

ground state through the $5s^25p5dnl$ and $5s5p^3nl$ channels in Fig. 4(b) and compare them with the experimental total recombination rate coefficient results in Fig. 4(a). The energy region is from 0 to 180 eV where all DR resonances associated with the $5p \rightarrow 5d$ and $5s \rightarrow 5p$ excitations are found. In the calculation, we did not include radiative recombination, which mainly contributes at low energy (0–15 eV). In order to obtain the DR rate coefficients, the DR cross section calculations were folded with the velocity distribution $f(v)$ given in Eq. (3) with the temperatures $kT_\perp = 0.1$ eV and $kT_\parallel = 1$ meV. In order to facilitate the comparison between the experimental and theoretical results, the latter were shifted until the peaks in the near-threshold region line up in energy with the experimental spectrum. The best agreement occurs when the whole theoretical spectrum was shifted by -3 eV. As indicated above, the overall error of the theoretical energy results is of about 5 eV. The agreement between experiment and theory is good for the energy region above 80 eV, which corresponds to the $5s^25p5dnl$ resonances. The experimental data exhibits structures, mainly at low energies, that are not accounted for theoretically by this two-channel calculation. Additional DR calculations for the $5s^25p^2nl$ channel were performed and show that besides the first peaks at an energy value of 8 eV, corresponding to $n=9$, the rest of the complex contributes with less than 1 Mb to the total cross section (see Fig. 2 for comparison). The other channels listed in Eq. (7) [$5s^25p5fnl$ ($n \geq 6$) and $5s5p^25dnl$ ($n \geq 6$)] contribute with less than 2 Mb to the total DR cross section, excluding the very-low-energy part, in which some resonances occur at a small value of E_c, producing a strong peak in the DR cross section.

We also present the results of the total DR rate coefficient $\langle v\sigma \rangle$ through the $5s^25p5dnl$ and $5s5p^3nl$ channels calculations from a statistical mixture of levels in the ground configuration in Fig. 4(c) and compare them with the pure ground-state calculations and experiment. The first excited level $5s^25p^2\ ^3P_1$ (level 2 in Table I) can radiate to the ground state by an $M1$ transition and has a lifetime of about 0.6 μs. The next excited level, $5s^25p^2\ ^1D_2$ (level 3 in Table I), radiates to the ground state by an $E2$ transition, and has a lifetime of about 5.3 μs. The time of flight of the ions from the production to the merging section of the experiment can be determined from the energies of the ions of 5.96 MeV/amu and a path of 120 m, which gives a travel time of about 4 μs. Since the ground configuration metastable fraction in the ion beam could not be determined experimentally, we calculate the DR cross section for the limiting case in which the ground state and the first two excited levels are statistically populated. In this case the threshold energies are slightly different; therefore, the whole theoretical spectrum of Fig. 4(c) was shifted now by -0.5 eV in order to obtain agreement with the experimental results in the near-threshold energy region. The theoretical spectrum constructed by assuming statistical populations in the metastable levels lines up in energy with the experimental spectrum and the shape of the resonance structures are quite similar, especially at the higher energies. The agreement between experimental and theoretical results seems to be better for the statistical mixture of levels in the ground configuration than for only the ground state. Figure 5 displays the same spectra as Figs. 4(a)
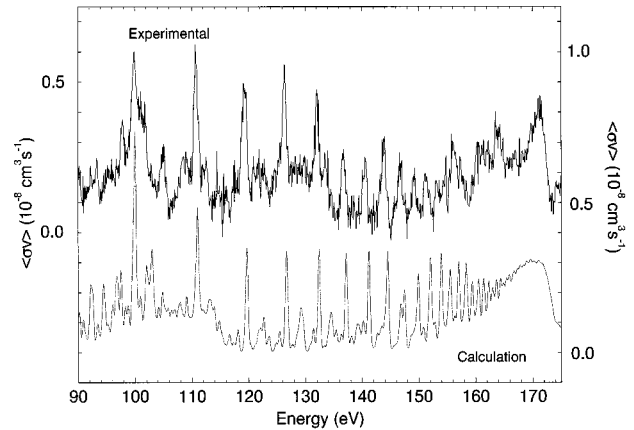

FIG. 5. Same as Figs. 3(a) and 3(b), except enlarged to show the energy region from 90 to 180 eV, in which the main features of the experimental spectrum are well identified. For clear presentation the ordinate axis is shifted, the left axis corresponding to the experimental spectrum (upper curve) and the right axis to the theoretical spectrum (lower curve), respectively.

and 4(c), but only over the 90–180 eV energy region in which the main features of the experimental spectrum are well identified. Caution must be exercised, however, in making a peak to peak comparison between theory and experiment in Fig. 4. We found that both small changes in the energy position of the doubly excited states and small changes in the convolution energy width led to large changes in the height of some of the peaks found in the spectrum of Fig. 4. In addition, we also solved the population time evolution equations for both the first 7 levels and for the first 15 levels, assuming that just in the production the population of the levels is statistically distributed and then allowing the levels to radiatively decay to the other levels. The results show that the first 3 levels very rapidly become the only levels populated, with a constant population (statistically) until a time of about 0.1 μs. Assuming that both the time of flight and the radiative rate coefficients were determined accurately, the calculated population is approximately 30% in the third level and 70% in the ground state. However, the DR calculations assuming this population distribution do not reproduce well the experimental data.

V. SUMMARY

We have employed a distorted-wave isolated-resonance and independent-process approximation to calculate dielectronic recombination cross sections for U^{28+} ion by using the AUTOSTRUCTURE codes in a semirelativistic mode. We have found that the cross sections calculated using this method are in good agreement with these calculated using the HULLAC codes in a fully relativistic mode. We compared the calculated cross sections with the experimental measurements obtained from the single-pass merged-beam experiments carried out at the UNILAC of GSI. A threshold energy transformation method was used to identify the different Rydberg series in the experimental spectrum. Theory and experiment agree reasonably well for the region 80–180 eV. At low energies, overlapping and possibly interacting reso-

nances makes identification of even Rydberg series limits very difficult. The low-energy spectrum is further complicated by energy uncertainties and the possible presence of unknown fractions of metastable levels. Which particular dielectronic recombination resonances are found just above threshold and how they interfere with the radiative recombination background for U^{28+} still remain a mystery.

[1] *Recombination of Atomic Ions*, Vol. 296 of *NATO Advanced Study Institute, Series B: Physics*, edited by W. G. Graham, W. Fritsch, Y. Hahn, and J. A. Tanis (Plenum, New York, 1992).

[2] Second Euroconference on Atomic Physics with Stored Highly Charged Ions, edited by R. Schuch, E. Lindroth, and H. Jürgen Kluge [Hyperfine Interact. **108**, 149 (1997)].

[3] A. Lampert, A. Wolf, D. Habs, J. Kenntner, G. Kilgus, D. Schwalm, M. S. Pindzola, and N. R. Badnell, Phys. Rev. A **53**, 1413 (1996).

[4] W. Zong, R. Schuch, E. Lindroth, H. Gao, D. R. DeWitt, S. Asp, and H. Danared, Phys. Rev. A **56**, 386 (1997).

[5] D. Savin, T. Bartsch, M. H. Chen, S. Kahn, D. Liedahl, J. Linkemann, A. Müller, S. Schippers, M. Schmitt, D. Schwalm, and A. Wolf, Astrophys. J. **489**, L115 (1997).

[6] S. Schennach, A. Müller, M. Wagner, J. Haselbauer, O. Uwira, W. Spies, E. Jennewein, R. Becker, M. Kleinod, U. Pröbstel, N. Angert, J. Klabunde, P. H. Mokler, P. Spädtke, and B. Wolf, in *Atomic Physics of Highly Charged Ions*, edited by E. Salzborn, P. H. Mokler, and A. Müller (Springer, Berlin, 1991), p. 205.

[7] Y. Hahn, Adv. At. Mol. Phys. **21**, 123 (1985).

[8] N. R. Badnell, J. Phys. B **19**, 3827 (1986).

[9] N. R. Badnell and M. S. Pindzola, Phys. Rev. A **39**, 1685 (1989).

[10] R. D. Cowan and D. C. Griffin, J. Opt. Soc. Am. **66**, 1010 (1976).

[11] J. Oreg, W. H. Goldstein, M. Klapisch, and A. Bar-Shalom, Phys. Rev. A **44**, 1750 (1991).

[12] M. Klapisch, J. L. Schwob, B. S. Fraenkel, and J. Oreg, J. Opt. Soc. Am. **67**, 148 (1977).

[13] S. Schennach, A. Müller, O. Uwira, J. Haselbauer, W. Spies, A. Frank, M. Wagner, R. Becker, M. Kleinod, E. Jennewein, N. Angert, P. H. Mokler, N. R. Badnell, and M. S. Pindzola, Z. Phys. D **30**, 291 (1994).

[14] C. Froese Fischer, Comput. Phys. Commun. **64**, 369 (1991).